TEST STAND FOR PROPELLERS AND ROTORS IN VTOL DRONE SYSTEMS

Małgorzata Wojtas[1]* iD, **Przemysław Wyszkowski**[2] iD, **Mirosław Mądro**[2] iD, **Maciej Osiewicz**[1] iD and **Paweł Kmita**[2] iD

[1] Aviation Propulsion Systems Department, Unmanned Technologies Center, Mechanics & Thermal Section, Łukasiewicz Research Network – Institute of Aviation, Al. Krakowska 110/114, 02-256 Warsaw, Poland
[2] Aviation Propulsion Systems Department, Unmanned Technologies Center, Hybrid Drives Section, Łukasiewicz Research Network – Institute of Aviation, Al. Krakowska 110/114, 02-256 Warsaw, Poland

Abstract

The paper proposes a stand that can be used for the testing of propellers and rotors with diameters up to 2.4 m, whose areas of application encompass, inter alia, vertical takeoff and landing (VTOL) type multi-rotor drone systems. The presented solution allows for testing propellers in systems with electric motors. To a certain extent, it is possible to achieve an increase in the measuring range by changing electric motors, power supply systems and measuring sensors. The paper presents several solutions for test stands that can be applied in the testing of propeller parameters, and commercially available propellers have also been deployed in the testing routines. The paper briefly presents the concept of the stand and its design, as well as the principle of operation and structural calculations underlying its functioning, after which the numerical model of the test stand is explained. The article then demonstrates the particular results of the test stand model's functioning using the EMRAX 188 electric motor and two propellers, namely a commercial Aerobat propeller and a composite propeller designed and manufactured at the Łukasiewicz – Institute of Aviation. Thus, the paper presents both the theoretical results that follow from the model and the results of experimental research.

Keywords: synchronous motors; numerical model; VTOL; propeller; test stand
Type of the work: research article

1. INTRODUCTION

In the coming years, immense progress is anticipated in relation to research on all-electric and hybrid-electric powered vertical takeoff and landing (eVTOL) aircraft, and it is expected that the primary focus of this research would be on non-helicopter VTOL aircraft large enough to carry passengers but yet not needing the conventional helicopter flight controls. Electric propulsion opens up the VTOL aircraft design space by harnessing concepts such as distributed electric propulsion (DEP) as well as facilitating new approaches to wingborne VTOL. Other advantages of electric propulsion include lower vibration and noise, less greenhouse gases emission, easier control and increased safety. The biggest factor hampering the development of aviation electrification is the energy density of energy storage. Even unmanned aerial vehicles using permanent magnet motors and a lithium polymer battery have a relatively short flight time. Therefore, a lot of research is conducted in order to develop technology which would enable an increase in flight range for airborne vehicles that use fuel cells [1].

The paper presents a test stand for measuring propeller characteristics in a system with an electric motor. The presented test stand was prepared as a part of the Axial Flux Synchronous Motors Test Stand described in the literature [1]. The stand is designed to provide information on the operating characteristics of the propeller, and to measure the dynamics of the propeller electric motor system. The response time of the propeller–electric motor configuration is one of the factors in assessing the system controllability.

To begin with, the authors present several solutions of commercial propeller thrust test stands. Next, design stages of propeller characteristic test stand (construction, structural analyses) are discussed. Furthermore, a numerical model of the test stand is presented and discussed in detail. Finally, the research conducted, in terms of applying the developed test stand to the particular case of two propellers, namely a wooden propeller (commercial, Aerobat [2]) and a composite propeller designed and manufactured at the Łukasiewicz – Institute of Aviation, is discussed. The propellers were tested with the EMRAX 188 synchronous motor [3].
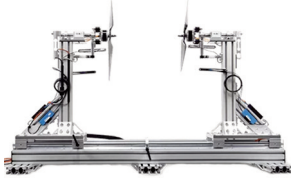
The prototype composite propeller was designed as a combination of two composite blades connected with an aluminium hub. The hub was designed in such a way that it allows determination of the propeller blades' angle of attack. Prepregs technology (involving reinforcement saturated with a strictly defined amount of uncured saturating mixture) was used for the manufacturing of the propeller blade. The blade structure consists of a spar with an upper and lower sheathing glued to it. The space between the sheathings is filled with a special foam. The covers and the spar are made with carbon fabrics and tapes. A perusal of the literature [4–6] would present more information on propellers in the manufacture of which similar compositions and manufacturing modi operandi have been used. It needs to be pointed out that carbon composites, e.g. carbon fibre reinforced epoxy (CFRE), carbon fibre reinforced polymer (CFRP), prepregs or carbon reinforced aluminium laminates (CARALL), are increasingly gaining importance in General Aviation and Small Aviation, as indicated in the literature [7]. The development of new technologies entails the development of research methods and numerical analyses as well as tools in the form of mathematical models.

2. TEST STANDS OVERVIEW

This section presents several solutions of commercial propeller test stands, as well as those of test stands provided by research facilities. Table 1 briefly summarises a few test stands similar to the one discussed in this article. The table summarises test stands' most important parameters and lists the units that have these stands at their disposal.

Table 1. Test stand overview [8–10].

Test Stand	Thrust	Torque	Propeller diameter	Electric parameters	RPM
 LY-70KGF Thrust Stand and Dynamometer **Wing Flayng**	±70 daN	±50 Nm	Max ~1.52 m	Current: 0–300 A Voltage: 5–110 V	60,000 – 150,000 RPM

 WF-CO-30KGF Coaxial Thrust Stand **Wing Flayng**	±30 daN	±20 Nm	Max ~1.00 m	Current: 0–150 A Voltage: 5–65 V	60,000 – 150,000 RPM
 Series 1780 Test Stand **TYTO Robotics**	±75 daN	±48 Nm	Max ~1.77 m	Current: 0–500 A Voltage:0–100 V	100,000 RPM
 Modular Stand for testing aircraft electric propulsion systems **NASA**	±225 daN	±200 Nm	Max ~1.77 m	N/A	20,000 RPM
 Rotor/propeller test stand in Hover **Institute of Aviation**	±3,000 daN	±4,800 Nm	Max ~10 m	Electric power: 315 kW	Min. 126 RPM, max. 1,500 RPM

3. PROPELLER TEST STAND

Experience shows that bench tests exercise a significant impact on the prototyping process. The research that has hitherto been conducted into helicopter and gyroplane rotors at Whirl Tower stands allows a lot of information to be obtained about the tested object and confirm the design assumptions. Additional information is available from the literature [11–13]. As indicated in the introduction to this study, the presented test stand is part of the Axial Flux Synchronous Motor Dynamometer, as well as the currently developed Hybrid (electric-combustion system) Dynamometer. The projects are carried out at the Aircraft Propulsion System Department at Łukasiewicz – Institute of Aviation. Work is being carried out to develop electric and hybrid drives (including fuel cells) targeted at unmanned systems and, in the future, air taxis.

3.1. Design

The measuring stand for testing the parameters of propellers and rotors in the hover was made as one of the stages of the Hybrid Drive Dynamometer project. The discussed test stand (Fig. 1) allows for testing propellers and rotors with diameters up to 2.4 m, and it can be used, inter alia, in VTOL type multi-rotor drone systems. This solution allows for testing propellers in systems with electric motors. To a certain extent, it is possible to achieve increases in the measuring range by changing electric motors, power supply systems and measuring sensors.

Fig. 1 below shows the thrust test stand and its simplified design and components, where the following nomenclature applies: 1 – propeller mounting hub, 2 – bearing assembly, 3 – torque metre carriage, 4 – torque sensor, 5 – electric motor, 6 – electric motor carriage, 7 – swivel joint, 8 – thrust sensor, and 9 – mounting frame.
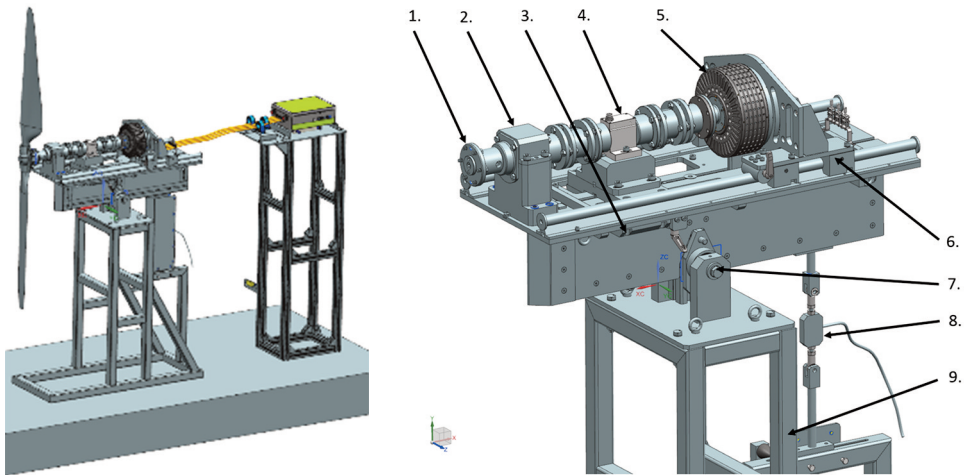

Figure 1. Propeller thrust test stand – visualisation [own elaboration].

The measurement of thrust on the stand is based on the method of balancing the moments as shown in Fig. 2. This type of method allows maximisation of the efficiency of the entire team and avoids the need to use correction factors. During test stand calibration, it was ensured that the position of the gauge sensor was set in such a way that the forces F1 and F2 were equal.
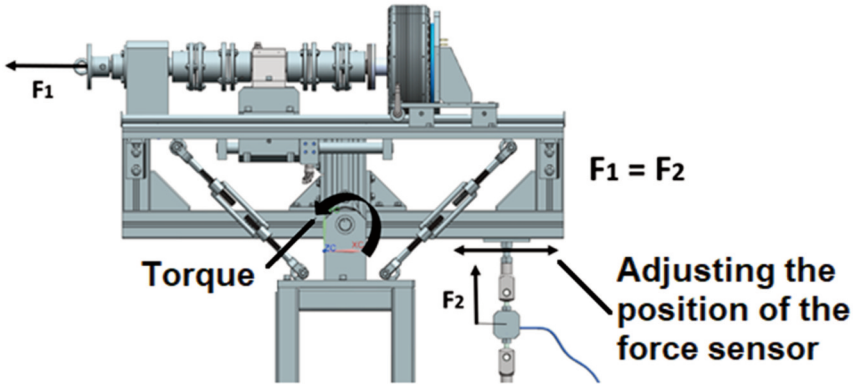
Figure 2. The principle of measuring the propeller thrust on the presented stand [own elaboration].

3.2. Structural analysis

The designed stand should meet a number of requirements in terms of structural strength and stiffness of the entire assembly. For this purpose, already at the design stage, several numerical analyses were carried out to check whether any of the designed elements would not be damaged prematurely.

The propeller shaft is subjected to a load that changes on both sides (bending and torsion). Its damage would result in damage to the propeller, station and safety elements. Based on successive computational iterations, a shaft with the smallest diameter of 30 mm was designed. The shaft has a hole to prevent the hub from sliding off the shaft during propeller operation. Therefore, calculations were made with the use of classic strength methods aimed at estimating the concentration of stresses in the described place. First, the tangential stresses were calculated for the maximum torque, i.e. 100 Nm, assumed for the test stand. The torsional stress in this cross-section is 18.87 MPa, and considering the workload concentration that is influenced by the diameter of the transverse hole and the dimensionless coefficient of unevenness of the electric motor operation at the level of 1.5, the stress at the level of 83.51 MPa was obtained. The next step was to carry out numerical calculations, to confirm the result obtained by using computations employing the classical method. For this purpose, the ANSYS computing environment with 'Static structural' module was used. Calculations were made based on the imported model and its discretisation as well as the assumed boundary conditions. The map of the material stress for the Huber-Von-Mises hypothesis is presented in Fig. 3.
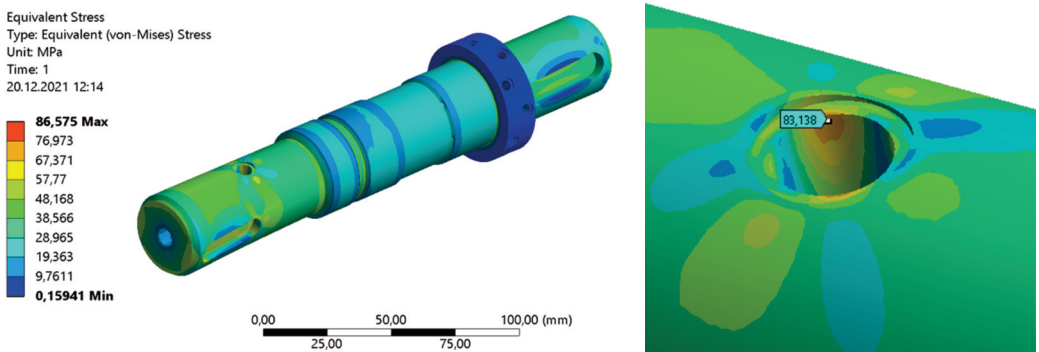

Figure 3. Map of reduced stress according to the Huber-Von-Mises hypothesis with a point measurement in the vicinity of the calculated transverse opening [own elaboration].

The comparison of the results showed a high convergence. Based on the analysis of the results in terms of fatigue strength, the 40HM material was selected.

The second element having a direct impact on the operational safety of the entire unit was the mounting plate. Its load depended on the value of the twisting moment and the thrust generated by the propeller. Due to the fact that it was a complex set of forces, calculations were made immediately using numerical methods. Based on the model previously prepared and imported to ANSYS, discretisation, assumption of contact conditions and definition of contacts between elements were carried out. The material strain map is shown in Fig. 4 according to the Huber-Von-Mises hypothesis.
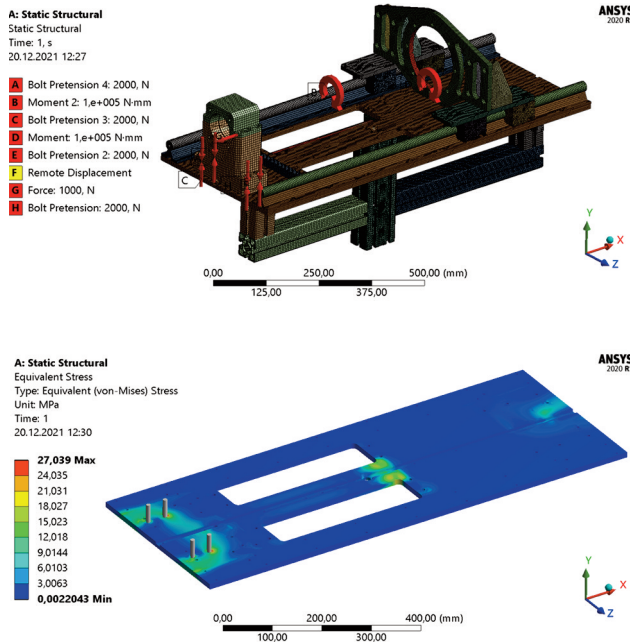

Figure 4. Structural calculation: (top) mounting plate model; (bottom) map of the mounting plate effort according to the Huber-Von-Mises hypothesis [own elaboration].

3.3. Electric diagram

Fig. 5 shows a general electrical diagram of the stand supply. The tested propeller is driven by an electric motor (in this case EMRAX 188) – MOT-1, which is connected to the tested object (rotor/propeller) by means of couplings and a torque sensor – B5. The electric motor is controlled by the BAMOCAR D3 – INV1 inverter, which is powered by a bidirectional voltage source 500 V/120 A/18 kW – U1. The inverter is liquid-cooled via the water–air heat exchanger – HE-420. All measurements are transferred to the HMI via NI's cRIO-based data acquisition system – MC. The application, installed on a PC, is an interface for the exchange of information between the operator and the system and enables the preview of the measured values. The inverter is controlled by the control panel (P1) next to the operator. The safety system is handled by the safety box (SC), in which there is a safety relay that disconnects the PWM output signal of the inverter's DC power.
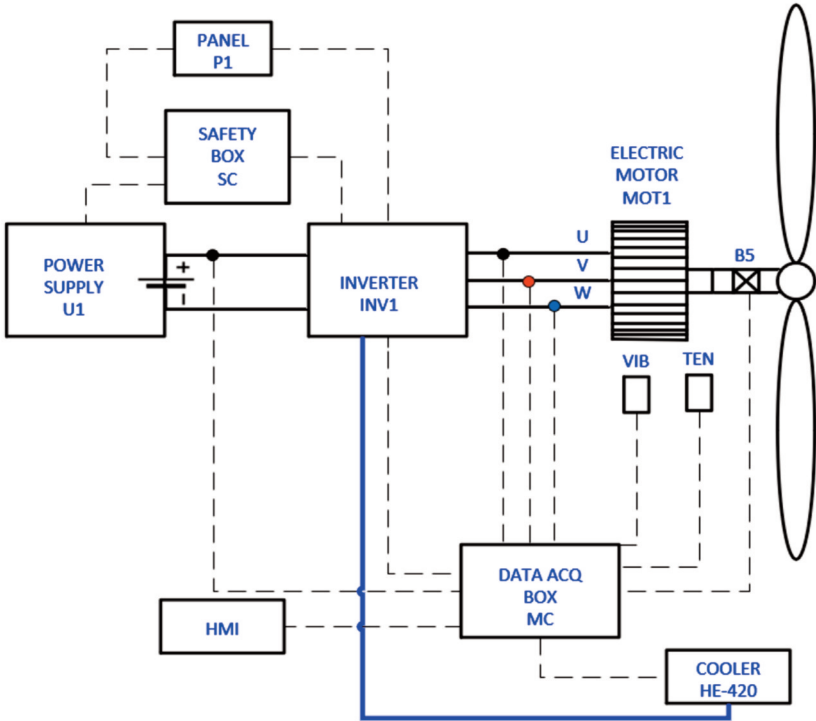
Figure 5. Propeller thrust test stand – electrical diagram [own elaboration].

3.4. Numerical model

The general model of the dynamics of the test stand for testing rotors and propellers, discussed in Section 3.4, is presented below (Fig. 6).
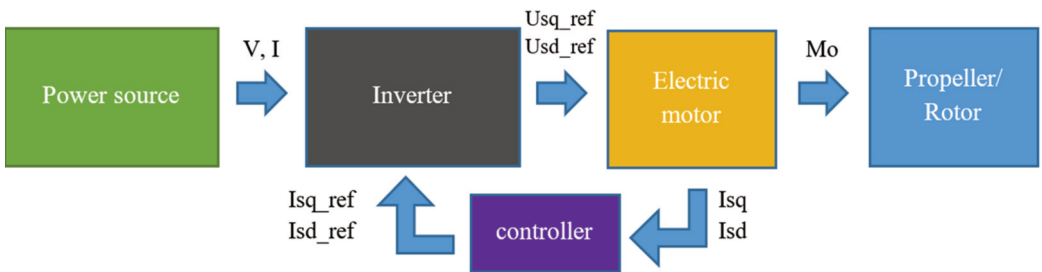
Figure 6. Dynamic model – block diagram [own elaboration].

In the dynamic model design, all major components of the device (test stand) are considered. The following blocks from the diagram shown are discussed below.

3.4.1. Electric motor mathematical model

Permanent magnet synchronous motors (PMSM) in some classifications are divided into PMSM sinusoidal electromotive force motors and trapezoidal electromotive force motors, also called brushless DC motors (BLDC) [14]. For applications where high dynamics, low electromagnetic torque pulsations and a large speed range are required, the PMSM motor is the best choice. The basic dependencies and equations describing a PMSM are as follows:

$$u_d = R_s i_d + \frac{d\psi_d}{dt} - p\omega_m \psi_q \tag{1}$$

$$u_q = R_s i_q + \frac{d\psi_q}{dt} - p\omega_m \psi_d. \tag{2}$$

The equations that bind the magnetic fluxes are:

$$\psi_d = L_{sd} i_d + \psi_f \tag{3}$$

$$\psi_q = L_{sq} i_q + \psi_f \tag{4}$$

where u_d, u_{do}, u_{dd}, u_q, u_{qo}, u_{qq}, i_d, i_q, L_s, R_s, and p, are, respectively, the voltages and currents in the rectangular coordinate system dq, inductances, resistances, flux from permanent magnets and the number of pole pairs. The electromagnetic moment can be determined from an approximate, where K_t is the structural constant:

$$M_e \cong \frac{3}{2} p\psi_f i_q \cong K_t i_q. \tag{5}$$

The equation of motion is analogous to the equations for the previously described devices and can be written in the form:

$$\frac{\omega_m}{dt} = \frac{1}{J_z}\left(M_e - M_o\right), \tag{6}$$

where ω_m, J_z and M_0 mean the angular velocity, equivalent moment of inertia of the engine and working devices, and the load moment, respectively. Based on the equations describing the synchronous device in a rotating rectangular coordinate system, a simulation scheme of the PMSM motor can be built.

3.4.2. Electric motor regulators

The basic regulation structure for a PMSM drive is shown in Fig. 7. Two control paths of the stator current components can be distinguished in the d and q axes, respectively. For motors with permanent magnets placed on the rotor surface, the value of the current in the d axis is set to 0. The current value in the q axis will then determine the electromagnetic moment developed in the motor. The implementation of the field-oriented control method requires the measurement of the angular velocity of the rotor and the currents in two phases.
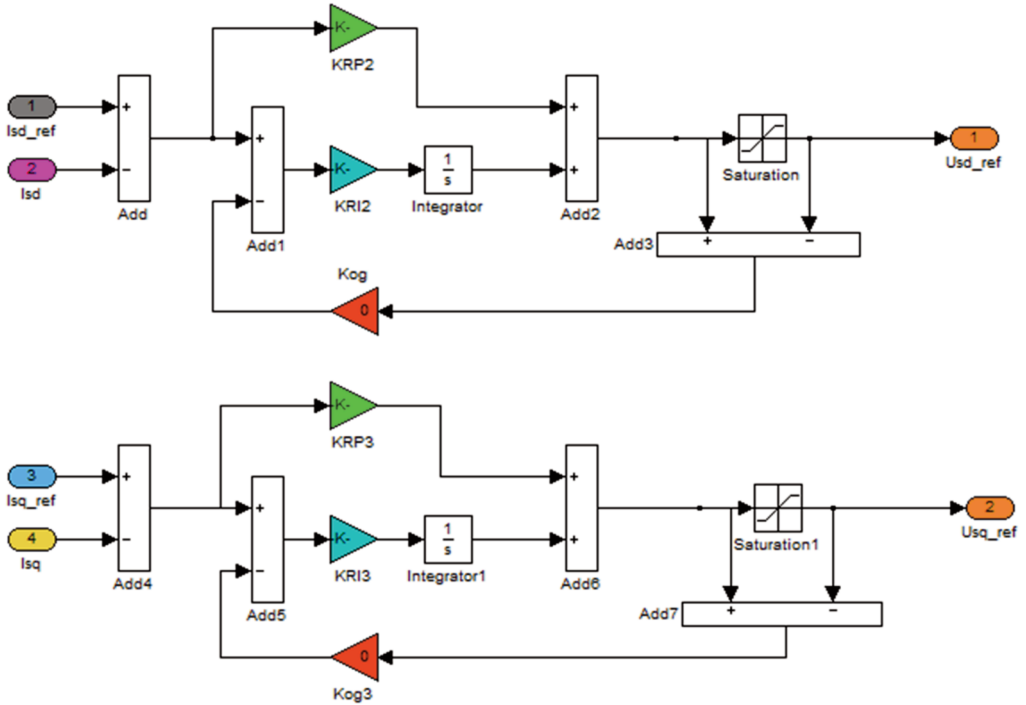
Figure 7. Construction of regulators in the MATLAB Simulink program [own elaboration].

The instantaneous values of the phase currents are first converted to a stationary rectangular frame of reference, and then, using the information on the angular position of the rotor gr, transformed to the rotating rectangular coordinate system xy (which will be referred to, alternatively, as the dq system). The current regulators in the d and q axes usually have the structure of a Proportional - Integral Controller (PI) [15].

3.4.3. Propeller model

When modelling the test object, we must consider the moments of inertia of the propeller, propeller hub and the shaft that transmits the engine torque to the propeller. Table 2 shows the values of the moments of inertia in consideration of the carbon composite Łukasiewicz – Institute of Aviation propeller.

Table 2. Moments of inertia of elements included in the model.

	I (*kg mm²*)
The knot from the engine to the propeller attachment	13,503
Propeller mounting hub	4,350
Propeller	246,083

Below, in Fig. 8, the propeller model design in the MATLAB Simulink environment is shown.
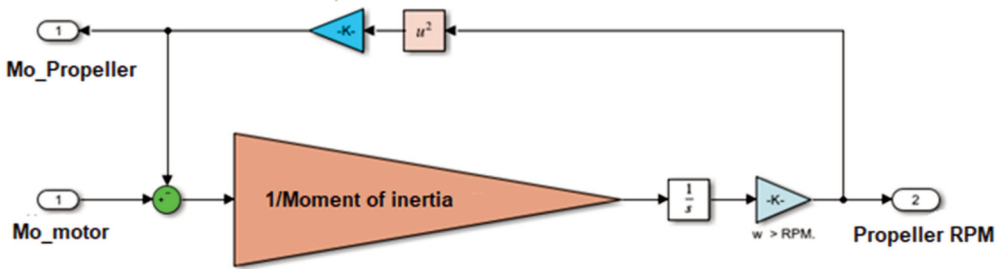
Figure 8. Propeller model with moments of inertia [own elaboration].

3.4.4. Complete test stand model

The electric motor model prepared in the MATLAB Simulink environment has been parameterised according to the technical specification of the EMRAX 188 HV AC engine. The technical specification mentions the dependence of the received torque on the given current, the EMRAX 188 electric motor has this relationship at the level of 0.6. This means that for every 1 A, we obtain 0.6 Nm. This relationship has been considered in the model (Fig. 9).
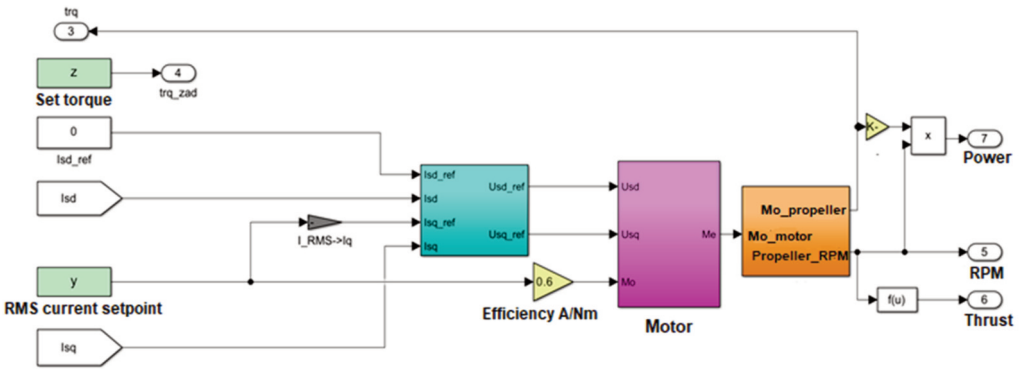
Figure 9. Model of the entire system built in MATLAB Simulink [own elaboration].

4. TESTS

In the first stage, tests have been carried out for the wooden Aerobat 54″ propeller, and the composite propeller made at the Łukasiewicz – Institute of Aviation with the EMRAX 188 electric motor. First, the stand with the Aerobat wooden propeller was tested. Tests were first performed to ascertain whether the test stand and the data acquisition system were working properly. After positive verification of the results, the characteristics of the wooden propeller were tested, and then the characteristics of the composite propeller (propellers are shown in Fig. 10).

At this stage of the research, the polar characteristics tests of the aforementioned propellers were performed. In parallel, tests were conducted to verify the numerical model described in the preceding section. The model tests concerned the dynamics of the propellers and the determination of the adjustment times. The values of torques and rotational speeds of propellers for the model and experimental tests were also compared. Below in Section 4.1, the test plan for the numerical model is presented.

Figure 10. Tests' propellers: commercial wooden Aerobat (left), and carbon composite
from the Łukasiewicz – Institute of Aviation (right).

4.1. Test plan

The control of the system during dynamic tests will be based on a step change of the torque of the electric motor. The input for the electric motor will be a current signal (reference current to flow through the motor windings), which is closely related to the motor torque.

The test plan is shown in the tables below (Table 3 – 1st cycle and Table 4 – 2nd cycle). The test is performed in two cycles: the 1st cycle is carried out for discerning small changes in the propeller torque, and the 2nd cycle for large ones.

Table 3. Initial parameters, step function of the torque and the corresponding currents – 1st cycle.

No.	Starting point – torque (Nm)	RMS current corresponding to torque (A)	Ending point – torque (Nm)	RMS current corresponding to torque (A)
1			8.5	14.2
2	6.0	10.0	10.0	16.7
3			14.0	23.3
4			25.5	42.5
5	23.0	38.3	27.0	45.0
6			31.0	51.7

7	33.0	55.0	35.5	59.2
8			37.0	61.7
9			41.0	68.3
10	45.0	75.0	47.5	79.2
11			49.0	81.7
12			53.0	88.3
13	58.0	96.7	60.5	100.8
14			62.0	103.3
15			66.0	110.0
16	68.0	113.3	70.5	117.5
17			72.0	120.0
18			76.0	126.7

Table 4. Initial parameters, step function of the torque and the corresponding currents – 2nd cycle.

No.	Starting point – torque (Nm)	RMS current corresponding to torque (A)	Ending point – torque (Nm)	RMS current corresponding to torque (A)
1	6.0	10.0	76.0	126.7
2	23.0	38.3		
3	33.0	55.0		
4	45.0	75.0		
5	58.0	96.7		
6	68.0	113.3		

The values given in the tables above have been assumed for the composite propeller. The maximum torque values are different for the two propellers as they have different characteristics and different moments of inertia. For this reason, the wooden propeller achieves a higher rotational speed. The manufacturer of the wooden propeller states that this propeller can reach a maximum rotational speed of 3,500 rpm, and above this speed, the propeller may be damaged.

4.2. Aerobat propeller – numerical model

4.2.1. Step function

The charts shown below (Fig. 11) represent the test sequence for step function, for the Aerobat wooden propeller, in the 1st and 2nd test cycles.
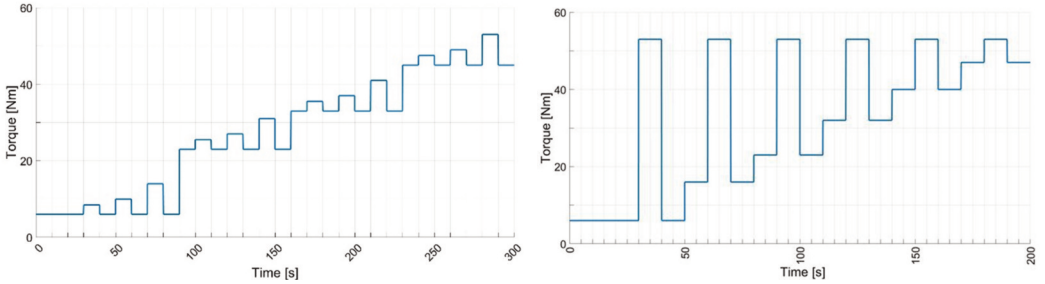
Figure 11. Course of step excitations for: 1st cycle (left) and 2nd cycle (right) [own elaboration].

4.2.2. Model tests results

The results of the wooden propeller tests in the numerical model for the step input function are presented below. In the chart immediately below (Fig. 12) are presented the responses of the propeller torque and rotational speed, to small step function, for different values of initial parameters (1st cycle). The subsequent chart (Fig. 13) shows the same parameters but in the next (2nd) test cycle, for large step function changes.

Figure 12. Summary of Aerobat propeller rotational speed and torque in the 1st cycle [own elaboration].

Figure 13. Summary of Aerobat propeller rotational speed and torque in the 2nd cycle [own elaboration].

The propeller–electric motor responses are shown in the tables below. Table 5 shows the adjustment time of the system to the step function in the 1st cycle, while Table 6 in the 2nd cycle. The adjustment time of the system (propeller–electric motor) is the time from maximum torque step application to the moment when the propeller has reached the given torque.
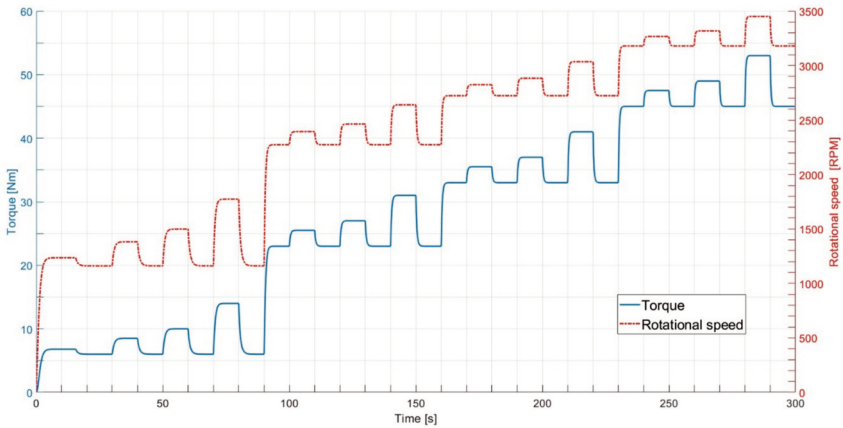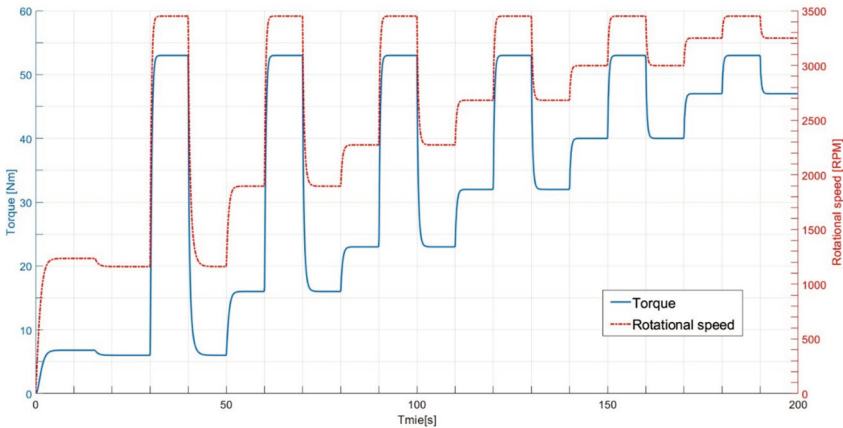
Table 5. Adjustment time for Aerobat propeller – 1st cycle.

No.	Starting point – torque (Nm)	Ending point – torque (Nm)	Adjustment time (s)
1		8.5	3.9
2	6.0	10.0	3.9
3		14.0	3.9
4		25.5	2.5
5	23.0	27.0	2.5
6		31.0	2.5
7		35.5	2.1
8	33.0	37.0	2.1
9		41.0	2.1
10		47.5	2.0
11	45.0	49.0	2.0
12		53.0	2.0

Table 6. Adjustment time for Aerobat propeller – 2nd cycle.

No.	Starting point – torque (Nm)	Ending point – torque (Nm)	Adjustment time (s)
1	6.0	53.0	2.5
2	16.0	53.0	2.4
3	23.0	53.0	2.3
4	32.0	53.0	2.3
5	40.0	53.0	2.2
6	47.0	53.0	2.0

4.2.3. Experiment/model comparison

In Table 7 and the chart (Fig. 14) beneath it, a comparison of the results from the model with the results from the test bench is presented. The results are given for the carbon composite Łukasiewicz – Institute of Aviation propeller. In Table 7, the results of the experimental tests and the tests on the model are compiled with the RMS current of the EMRAX 188 electric motor. The presented results pertain to the tests of propeller polar characteristics.

Table 7. Comparison of actual results with the simulation results for the same RMS currents, Aerobat propeller.

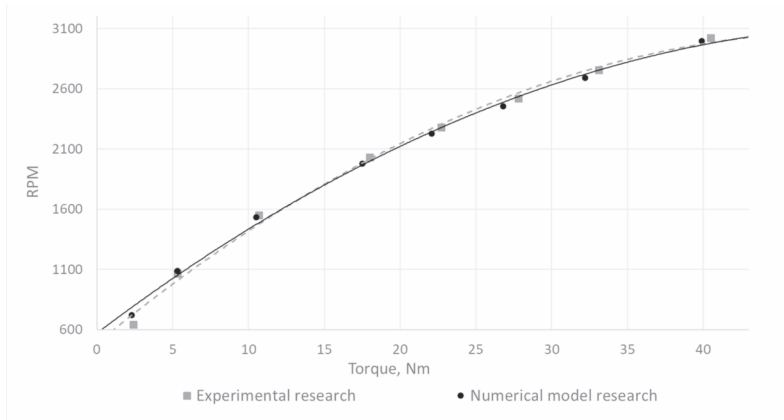|	Experimental research		Numerical model research	
Current (A)	**Torque (Nm)**	**Rotational speed (RPM)**	**Torque (Nm)**	**Rotational speed (RPM)**
3.86	2.4	640.0	2.3	720.0
8.76	5.3	1,065.0	5.3	1,087.0
17.45	10.7	1,550.0	10.5	1,534.0
29.08	18.0	2,030.0	17.5	1,980.0
36.80	22.7	2,280.0	22.1	2,226.0
44.70	27.8	2,520.0	26.8	2,456.0
53.6	33.1	2,755.0	32.2	2,688.0
66.5	40.5	3,020.0	39.9	2,995.0

Figure 14. Comparison of actual results with the simulation results
for Aerobat propeller [own elaboration].

4.3. Composite propeller – numerical model results

4.3.1. Step function

The charts shown below (Fig. 15) present the test sequence for step function, for the carbon composite Łukasiewicz – Institute of Aviation propeller in the 1st and 2nd test cycles.
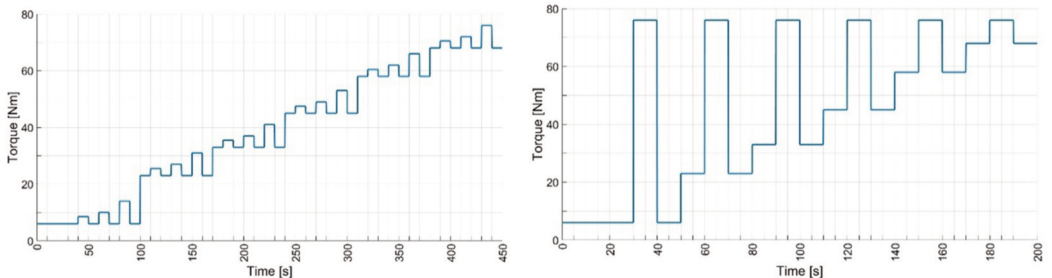

Figure 15. Course of step excitations for 1st cycle (left) and 2nd cycle (right) [own elaboration].

4.3.2. Model tests results

The results of the carbon composite Łukasiewicz – Institute of Aviation propeller tests in the numerical model for the step function are presented below. The chart below (Fig. 16) shows responses of the propeller torque and rotational speed, to small step function, for different values of initial parameters (1st cycle). The subsequent chart (Fig. 17) shows the same parameters but in the next (2nd) test cycle, for large step function changes.
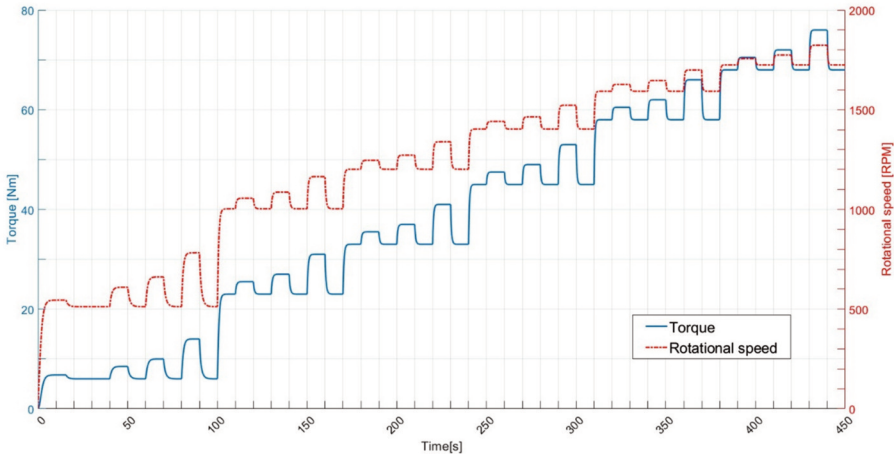
Figure 16. Summary of Łukasiewicz – Institute of Aviation propeller rotational speed and torque in the 1st cycle [own elaboration].
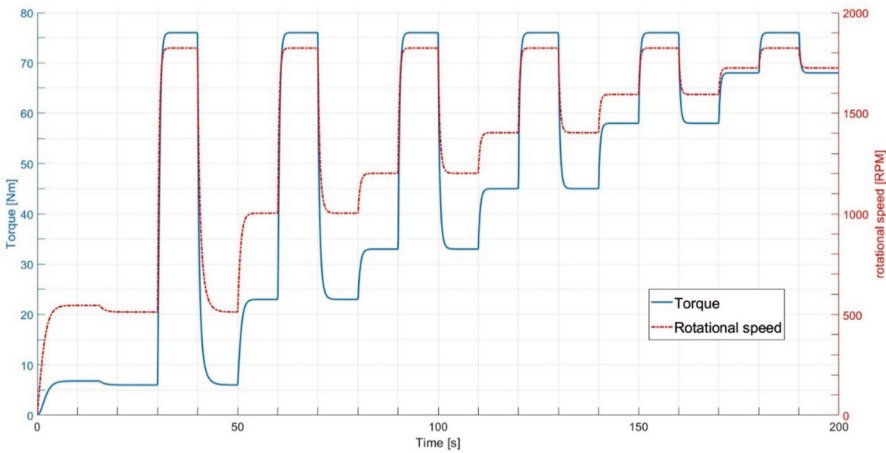
Figure 17. Summary of Łukasiewicz – Institute of Aviation propeller rotational speed and torque in the 2nd cycle [own elaboration].

The composite propeller–electric motor responses are shown in the tables below. Table 8 shows the adjustment time of the system to the step function in the 1st cycle, while Table 9 in the 2nd cycle. The adjustment time of the system (propeller–electric motor) is the time from maximum torque step application to the moment when the propeller has reached the given torque.

Table 8. Adjustment time for Łukasiewicz – Institute of Aviation propeller – 1st cycle.

No.	Starting point – torque (Nm)	Ending point – torque (Nm)	Adjustment time (s)
1	6	8.5	6.0
2		10.0	6.0
3		14.0	6.0
4	23	25.5	4.7
5		27.0	4.5
6		31.0	4.5
7	33	35.5	3.7
8		37.0	3.7
9		41.0	3.7
10	45	47.5	3.0
11		49.0	3.0
12		53.0	3.0
13	58	60.5	2.8
14		62.0	2.7
15		66.0	2.7
16	68	70.5	2.2
17		72.0	2.2
18		76.0	2.2

Table 9. Adjustment time for Łukasiewicz – Institute of Aviation propeller – 2nd cycle.

Lp.	Starting point – torque (Nm)	Ending point – torque (Nm)	Adjustment time (s)
1	6.0	76.0	3.4
2	23.0	76.0	3.1
3	33.0	76.0	3.0
4	45.0	76.0	2.9
5	58.0	76.0	2.8
6	68.0	76.0	2.2

4.3.3. Experiment/model comparison

In Table 10 below and the chart beneath it (Fig. 18), a comparison of the results from the model with the results from the test bench is presented. The results are given for the carbon composite Łukasiewicz – Institute of Aviation propeller. In Table 10, the results of the experimental tests and the tests on the model are compiled with the RMS current of the EMRAX 188 electric motor. The presented results pertain to the tests of propeller polar characteristics.

Table 10. Comparison between the actual results and the simulation results for the same RMS currents, for the carbon composite Łukasiewicz – Institute of Aviation propeller.

| Present current (A)	Experimental research		Numerical model research	
	Torque (Nm)	Rotational speed (RPM)	Torque (Nm)	Rotational speed (RPM)
11.09	7.62	565.0	6.65	540.0
23.99	15.35	825.0	14.39	794.0
38.96	24.40	1,045.0	23.38	1,011.0
54.32	33.37	1,215.0	32.69	1,195.0
63.99	38.73	1,305.0	38.39	1,296.0
75.37	45.15	1,405.0	45.22	1,406.0
89.29	52.30	1,515.0	53.57	1,531.0
103.81	59.35	1,615.0	62.29	1,651.0
121.99	66.91	1,715.0	73.19	1,789.0
137.16	72.61	1,770.0	82.30	1,897.0
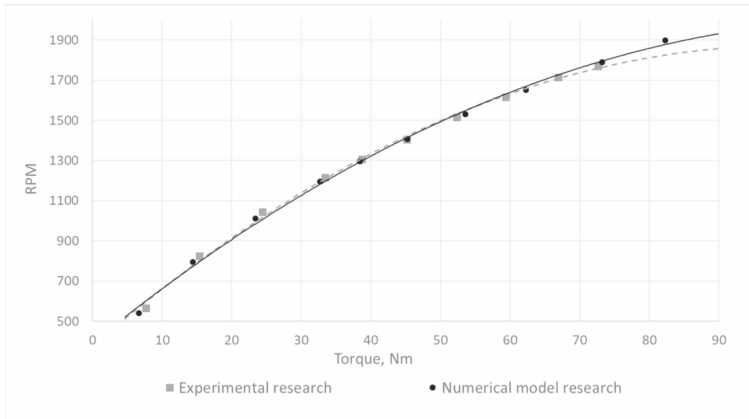
Figure 18. Comparison of actual results with the simulation results for the carbon composite Łukasiewicz – Institute of Aviation propeller [own elaboration].

5. CONCLUSION

The test stand presented in article was designed and manufactured with the intention of testing propellers in a system with electric motors. To a certain extent, the measuring range of the stand can be changed and adapted to a specific electric motor and propeller. Currently (without major changes in mechanical construction), in addition to the EMRAX 188 motor, it is possible to use the EMRAX 208.

In cooperation with the EMRAX 188 engine, the composite propeller is able to achieve the set torque. The rotational speeds of the propeller at given moments agree with the speeds of the propeller measured on the actual stand. The differences in the torque measured on the real stand and that measured in the simulation model at the same currents result from the fact that the simulation works

in ideal conditions, without disturbances, and some model elements are based on polynomials, which are not able to perfectly reflect the real conditions. Another reason may be inaccurate/rounded measurements of currents, torques and velocities on an actual test bench. The propeller response time (adjustment time), with increasing torque, and thus also with increasing power, needed to obtain the set torque value decreases.

As for the wooden propeller, in cooperation with the EMRAX 188 engine, it achieves the given torque in a shorter time than a composite propeller. The differences between the model and the real stand in the currents and the corresponding moments and velocities have the same causes as in case of the composite propeller.

Before moving on to summarising the results of the present study, attention needs to be drawn to fact that a coefficient of 0.6 was adopted for the numerical model, which is representative of the relationship prevailing between the current flowing through the motor winding and the torque. During measurements on the real stand, this ratio was not always 0.6, but it changed from ~0.7 for low currents to ~0.5 for high currents, although the values changed, with different values manifesting in different cycles.

Based on the above conclusions, we may ascertain that the EMRAX 188 engine possesses a power appropriate for achieving the set torques and speed, but that the duration of the adjustment is not satisfactory. Therefore, the next stage of the project will be to rebuild the model and test stand using a larger EMRAX 208 motor.

REFERENCES

[1]   Kędzierski, Ł., Sikorski, R., Wyszkowski, P. and Bartela, M. "Axial Flux Synchronous Motors Test Stand." *Przegląd Elektryczny* Vol. 97 No. 8 (2021): pp.121–127.

[2]   Available at: https://aerobat.es/en/.

[3]   Available at: https://emrax.com/.

[4]   Wojtas, M., Wyszkowski, P., Kmita, P. and Osiewicz, M. "Prototype Carbon Fibre Propeller Dedicated for Hybrid Power Unmanned Aerial Vehicles with MTOW up to 300kg." *48th European Rotorcraft Forum*. Switzerland, September 5–9, 2022.

[5]   Klimczyk, W.A. "Aerodynamic Design and Optimization of Propellers for Multirotor." *Aircraft Engineering and Aerospace Technology* Vol. 91 No. 1 (2022): pp. 21–30.

[6]   Kozaczuk, K. "Composite Technology Development Based on Helicopter Rotor Blades." *Aircraft Engineering and Aerospace Technology* Vol. 92 No. 3 (2018): pp. 273–284.

[7]   Seltak, L., Kowalik, R. and Łusiak, T. "Practical use of Composite Materials used in Military Aircraft." *Materials* Vol. 14 No. 17 (2021):p. 4812.

[8]   Available at: https://www.wingflyingtech.com/.

[9]   Available at: https://www.tytorobotics.com/.

[10]   Available at: https://www.techbriefs.com/component/content/article/tb/pub/briefs/propulsion/24843.

[11]   Wojtas, M., Czajkowski, Ł. and Szumański, K. "Ground Test Stand for Testing Rotors in Insulated Conditions." *Transactions on Aerospace Research* Vol. 262 No. 1 (2021): pp. 15–23.

[12]   Wojtas, M. and Czajkowski, Ł. "Prototype Test Stand for Testing Insolated Rotor Systems." *Journal of KONES Powertrain and Transport* Vol. 26 No. 3 (2019): pp. 257–264.

[13]   Wojtas, M., Czajkowski, Ł., Stanisławski, J. and Szumański, K. "Numerical Analyses of Different State of Flight of New Concept Coaxial Rotor Dedicated to Unmanned Helicopters." *45th European Rotorcraft Forum*: pp. 1472–1479, Vol. 1. Warsaw, September 17–20, 2019.

[14]   Zhao, J., Han, Q., Dai, Y. and Hua, M. "Study on the Electromagnetic Design and Analysis of Axial Flux Permanent Magnet Synchronous Motors for Electric Vehicles." *Energies* Vol. 12 No. 18 (2019): p. 3451.

[15]   Grzesiak, L.M. "Sterowanie napędów i serwonapędów elektrycznych." 2009. Available at: https://www.ee.pw.edu.pl/~purap/CUARPE/data/LMG_PRESKRYPT_czesc.pdf.